





Coexistence of low and high spin states in $\text{La}_{18}\text{Co}_{28}\text{Pb}_3$ Weiyi Xia ¹, Vladimir Antropov ^{1,2}, Yongxin Yao ^{1,2} and Cai-Zhuang Wang ^{1,2,*}¹*Ames National Laboratory, U.S. Department of Energy, Ames, Iowa 50011, USA*²*Department of Physics and Astronomy, Iowa State University, Ames, Iowa 50011, USA*

(Received 13 February 2024; revised 23 April 2024; accepted 4 June 2024; published 20 June 2024)

The electronic structure and magnetic properties of a newly predicted stable ternary compound $\text{La}_{18}\text{Co}_{28}\text{Pb}_3$ are studied using electronic structure analysis. The ground state of this compound is ferromagnetic, with three positions of nonequivalent magnetic Co atoms. A strong dependence of magnetic properties on volume shows that this system is situated near the point of magnetic instability. The coexistence of high- and low-spin ferromagnetic states as a function of volume near equilibrium was discovered. A corresponding spin tunneling splitting was estimated. The stability of the theoretically predicted magnetic ground state was tested by varying the Hubbard parameter. The thermal spin fluctuations were added to estimate the paramagnetic moment and a Curie temperature. The necessity of experimental verification of the obtained results is emphasized.

DOI: [10.1103/PhysRevB.109.214429](https://doi.org/10.1103/PhysRevB.109.214429)

Many solid-state systems exist near the point of magnetic instabilities [1]. These instabilities can be related to the appearances of both local magnetic moment and long-range magnetic order [2]. It has been shown that all these systems possess large amounts of spin fluctuations (SFs), which can be low-temperature quantum paramagnetic and high-temperature classical (thermal) local moment fluctuations [3,4]. All these fluctuations are essential for determining the right magnetic ground states and the thermal properties of paramagnets and ordered magnets. Significant SFs have been observed experimentally in such systems as Invar and anti-Invar alloys, magnetoresistive manganates, and numerous paramagnets (like Pd) [5]. A critical consequence of SFs for the superconductivity has also been observed in cuprates and iron pnictides [6,7]. The mechanism of SF-induced superconductivity in these materials still needs to be better understood. However, the presence of strong SFs appears to be an essential ingredient of such superconductivity. Therefore, searching for systems with strong SFs near the point of magnetic instability or quantum critical point (QCP) is a natural strategy for novel superconductor discovery. Such magnetic instability can be both ferromagnetic (FM) and antiferromagnetic (AFM) because the coexistence of FM/AFM and superconductivity has been established experimentally. However, the inclusion of SFs in the current electronic structure theories needs to be better established. While numerous theories of SFs have been proposed in the past, only a few connections between those theories and the physics of realistic materials have been established. While popular, the dynamical mean-field theory method still needs to be revised to the correct description of major figures of merits of metallic magnetism, such as Curie temperature and susceptibility [8].

To search for new materials, one may focus on ternary compounds containing immiscible pairs of elements, and if

one of them is magnetic (such as Co-Pb, Ba-Fe, etc.), one can hope to generate SF-rich systems. An immiscible pair, or “antagonistic pair,” is a pair of elements from which no existing binary phases have been observed in the phase diagram. Still, when such ternary compounds form, the immiscible elements are usually segregated from each other, with the third element encapsulating or separating them, thus leading to reduced dimensionality of the crystal structures [9]. When a $3d$ transition metal is forced to adopt such reduced dimensionality, complex electronic and magnetic states such as superconductivity [10] and fragile magnetism [11,12] can emerge.

Recently, a series of La-Co-Pb compounds containing an immiscible pair of Co and Pb was predicted using machine learning and first-principles calculation methods [13]. Among them, a ternary compound $\text{La}_{18}\text{Co}_{28}\text{Pb}_3$ was shown to be thermodynamically favorable below 200 K by comparing its Gibbs free energy with other competing phases. In this study, we investigate the electronic and magnetic properties of this compound. We show that the ground state of this ternary compound is ferromagnetic, with a QCP appearing under pressure. Multiple magnetic orderings, including FM and AFM phases, are revealed. The coexistence of high- and low-spin FM states around the equilibrium is predicted. The influence of SFs on magnetic properties obtained in the density functional theory (DFT) is studied in the frame of a rotationally invariant form of SF addition using a coupling constant integration formalism [14].

By SFs here, we assume not Hubbard-like Coulomb static correlations but temporal collective variables describing overdamped dynamically related SFs, paramagnons, and itinerant fluctuations of spin density not related to the local moment fluctuations, as schematically shown in Fig. 1. These fluctuations are missing in simplified approximations such as local density approximation (LDA) or generalized gradient approximation (GGA) for the exchange-correlation energy functionals. In addition, the coexistence of two or more magnetic states leads to the appearance of the spin tunneling

*Contact author: wangcz@ameslab.gov

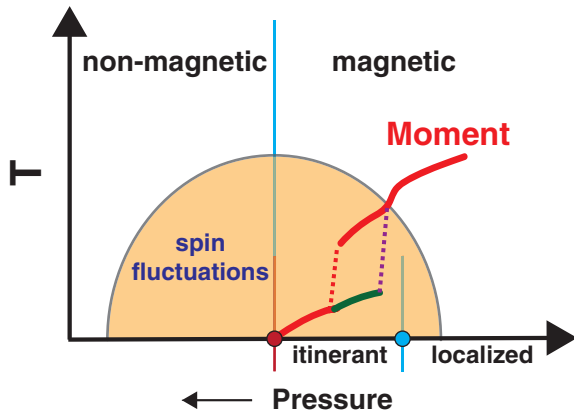


FIG. 1. Schematic diagram of spin fluctuations appearance near quantum critical point for the case of nonmagnetic \rightarrow itinerant magnetic \rightarrow localized magnetic transition as a function of pressure. The red dot corresponds to the Stoner (long-range order) criterion fulfillment, with the blue line separating magnetic and nonmagnetic states, while the blue dot corresponds to the local moment (Anderson) criteria fulfillment. An itinerant-localized transition is shown here with the coexistence of two different ferromagnetic solutions. The red line corresponds to the magnetization of the ground FM state, while the green line corresponds to the magnetization of the metastable low-spin FM state.

effect, which can change the overall stability of the magnetic states. Due to all these limitations, it has been shown that LDA/GGA methods substantially overestimate the tendency to magnetism at $T = 0$ K for the itinerant magnets (i.e., ZnZr₂, NiAl, iron pnictides, etc.) [15–17]. However, both LDA and GGA methods can identify systems near QCP. Below, we will demonstrate that the recently predicted La₁₈Co₂₈Pb₃ ternary compound can be considered a system near QCP.

The DFT calculations are performed by using the Perdew-Burke-Ernzerhof (PBE) exchange-correlation functional within the framework of GGA [18] as implemented in the Vienna *Ab initio* simulation package (VASP) [19,20]. A plane-wave cutoff energy is set to 520 eV, and the positions of atoms and the cell parameters are fully optimized. The accuracy of the electron self-consistent field is set to 10^{-4} eV, and the Brillouin zone is sampled using a set of gamma-centered uniform $8 \times 8 \times 6$ grids. The unit-cell shape (i.e., the three lattice vectors) and the atomic positions in the unit cell are fully relaxed by DFT calculations using the VASP code until the forces on every atom are less than 0.01 eV/Å.

I. ATOMIC AND ELECTRONIC STRUCTURES

The crystal structure of the La₁₈Co₂₈Pb₃ compound is shown in Fig. 2(a). It has a tetragonal lattice with an $I4/mmm$ space group symmetry with a complex unit cell containing 98 atoms. There are four Wyckoff sites for La ($4c$, $8i$, $16m$, $8j$), three Wyckoff sites for Co ($32o$, $16n$, $8h$), and two for Pb ($2b$, $4e$), respectively. Within the symmetrized unit cell, the atoms distribute several layers along the c direction. For each La layer, the La atoms form an inner ring with the center occupied by the Pb atom and four outer rings, which form multiple

tetrahedra with Co o and n sites. The four outer rings are then connected by an octahedron between each other with Co o and h sites. The lattice constants $a = 14.02$ and $c = 10.01$ Å are obtained after DFT optimization at the GGA-PBE level, with a c/a ratio of 0.714 close to $1/\sqrt{2}$. The ground state of this compound is FM, and the calculated formation energy is only 1 meV/atom above the known convex hull. This is calculated by comparing its formation energy with respect to the nearby three known phases on the convex hull, La₄Pb₃, La₆Co₁₃Pb, and La₁₂Co₆Pb. These three phases are located at the vertices of a triangle (called a Gibbs triangle), which enclose the composition of La₁₈Co₂₈Pb₃. This energy is used to assess the thermodynamic stability of La₁₈Co₂₈Pb₃ against decomposition into the nearby three known phases, suggesting that this compound could be synthesizable by experiment.

The total and partial density of states (DOS) is presented in Fig. 2(b). The positive and negative values represent the spin-up and spin-down components of the DOS, respectively. A prominent feature is the high density of states near the Fermi level for the minority spin, primarily originating from Co atoms, particularly the Co o site. The contrasting behavior between the spin-up and spin-down states near the Fermi level is evident in the spin-polarized band structures displayed in Fig. 2(c) for spin up and Fig. 2(d) for spin down. Notably, the DOS peak near the Fermi level is contributed from some flat bands, as depicted in Figs. 2(c) and 2(d), representing a Van Hove singularity.

We also calculate the differential electron density for the ground state to investigate the bonding interactions between La, Co, and Pb atoms. In Fig. 3, the atomic positions and the differential charge density are plotted in the ab plane [(a) and (b)] and in the ac plane [(c) and (d)] cutting through the center Pb atom. The formation of bonding interactions between the Pb atom and surrounding La atoms can be seen. No direct interactions between the Pb and Co atoms are observed. This charge density distribution is consistent with the experimental observation that Pb and Co cannot form any stable binary phases because there are no direct bondings between the Pb and Co atoms. Since both Pb and Co atoms can form bonds with La atoms, La atoms can serve as bridges to stabilize the ternary compound containing the immiscible pair of Pb and Co elements. The La atoms connect Pb and Co atoms with La-Pb and La-Co bonds to ensure the formalization and stabilization of this ternary compound involving Pb-Co immiscible pairs.

II. COMPETING MAGNETIC STATES

While the ground state of the La₁₈Co₂₈Pb₃ compound is FM with an average magnetic moment of $0.63 \mu_B$ per Co atom ($35 \mu_B$ per unit cell with two formula units), our calculations also reveal another FM state with a magnetic moment of only $0.20 \mu_B$ per Co atom ($11 \mu_B$ /cell). This state is achieved via structural relaxation with an initial moment on Co atoms of $1.5 \mu_B$ or less, with the same settings, which can be considered a local minimum. We refer to these two FM states as high-spin and low-spin FM states. In addition to the FM configurations, we found many AFM configurations. For simplicity, we investigate three AFM configurations: two $a - b$ in-plane antiferromagnets (AFM1 and AFM2) and one out-of-plane

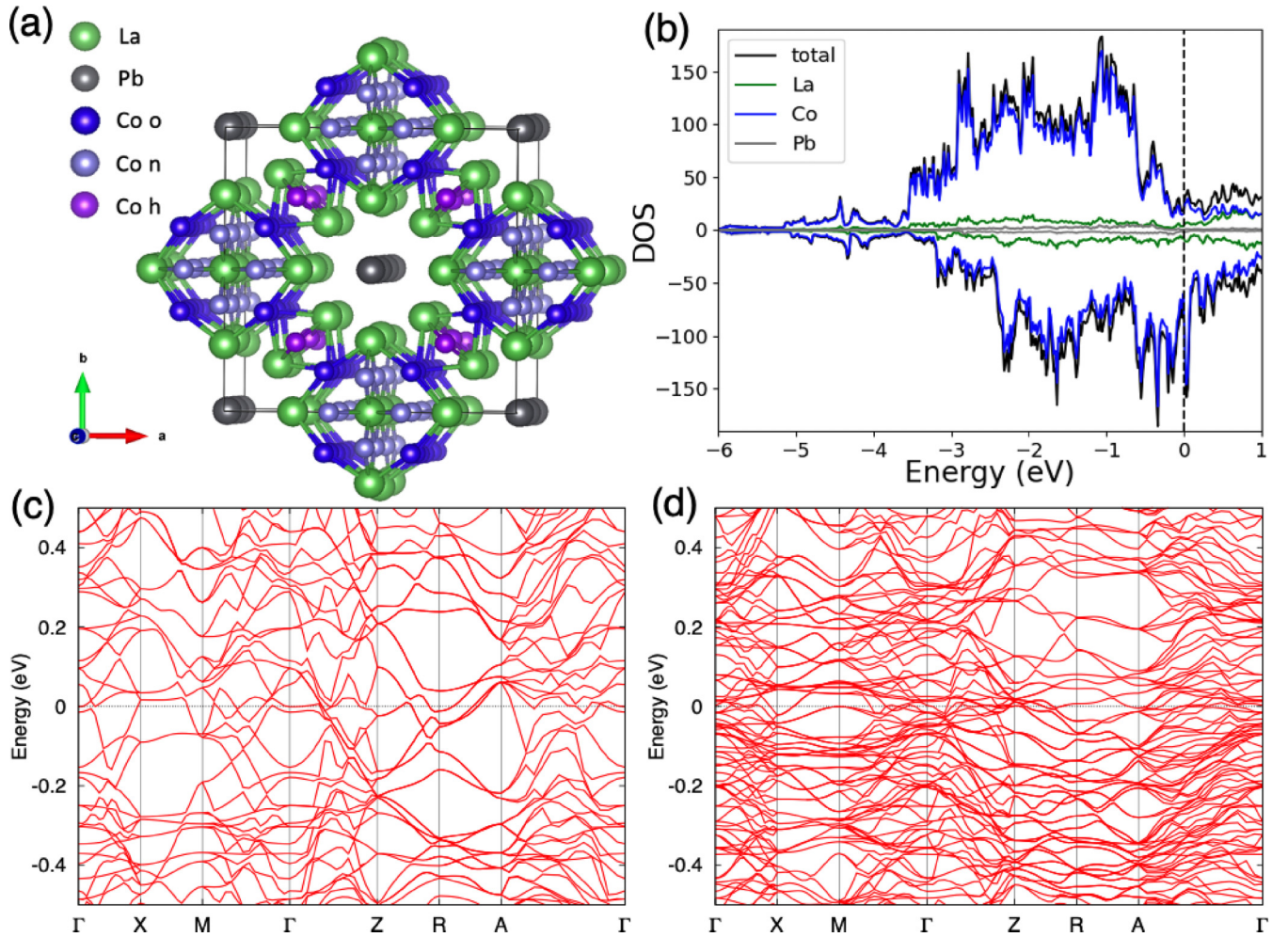


FIG. 2. (a) The crystal structure of the predicted $\text{La}_{18}\text{Co}_{28}\text{Pb}_3$ ternary compound. (b) The calculated density of states of the ferromagnetic ground state. We also show the calculated spin-polarized band structure around Fermi level (at 0 eV) for majority spin (c) and minority spin (d).

antiferromagnet (AFM3), as illustrated in Fig. 4(a). The total energies as the function of volume for these FM and AFM configurations are shown in Fig. 4(b). The total energies for the two FM states are close, with the energy difference within 18 meV per Co atom. The energies of the AFM configurations are higher than the high-spin FM state (but <18 meV per Co atom). Our results indicate that while the ground state is a high-spin FM state for $\text{La}_{18}\text{Co}_{28}\text{Pb}_3$, there are multiple competitive magnetic states within a small range around equilibrium volume. The energy difference between these states is within the 18 meV per Co atom range.

III. MAGNETIC PHASE TRANSITION

Now, we study the volume dependence of the magnetic moment for the low- and high-spin FM states, as shown in Fig. 4(c). The average magnetic moment per Co atom changes significantly from 0.2 to $0.6 \mu_B$ around the equilibrium volume. The magnetic moments for the three types of nonequivalent Co atoms at different volumes are also shown in Fig. 4(d). For Co *h* sites, the magnetic moment does not change much going from low to high spin state, while for *n* sites, a significant change is observed.

The hysteresislike loop for magnetization around the equilibrium volume in Figs. 4(c) and 4(d) is obtained by reducing (increasing) the volume from the high (low) spin state in a small increment and using the wavefunction from the previous volume as the starting wavefunction for the self-consistent DFT calculations. Our calculations suggest that the low and high spin states in $\text{La}_{18}\text{Co}_{28}\text{Pb}_3$ should be stable separately at a volume below $0.96V_0$ and above $1.04V_0$, respectively. Both states coexist in the volume range of $0.96-1.04V_0$. Figure 4(b) also shows the presence of other metastable collinear states in this region of volumes. The existence of such a hysteresislike loop for magnetization indicates a possible low- to high-spin phase transition under pressure.

By comparing the DOS near the Fermi level for high and low spin states, one can see a significant difference between two types of nonequivalent Co atoms, *o* and *n* sites, as shown in Figs. 4(e) and 4(f). Moving from the low to the high spin state, we observe a significant increase in the DOS of Co *o* and *n* atoms at the Fermi level for the minority and a significant decrease for the majority spin. The main peak position of the minority spin for all the nonequivalent Co sites shifts from unoccupied states to occupied states, indicating a significant change in the on-site exchange interactions for these Co *d*

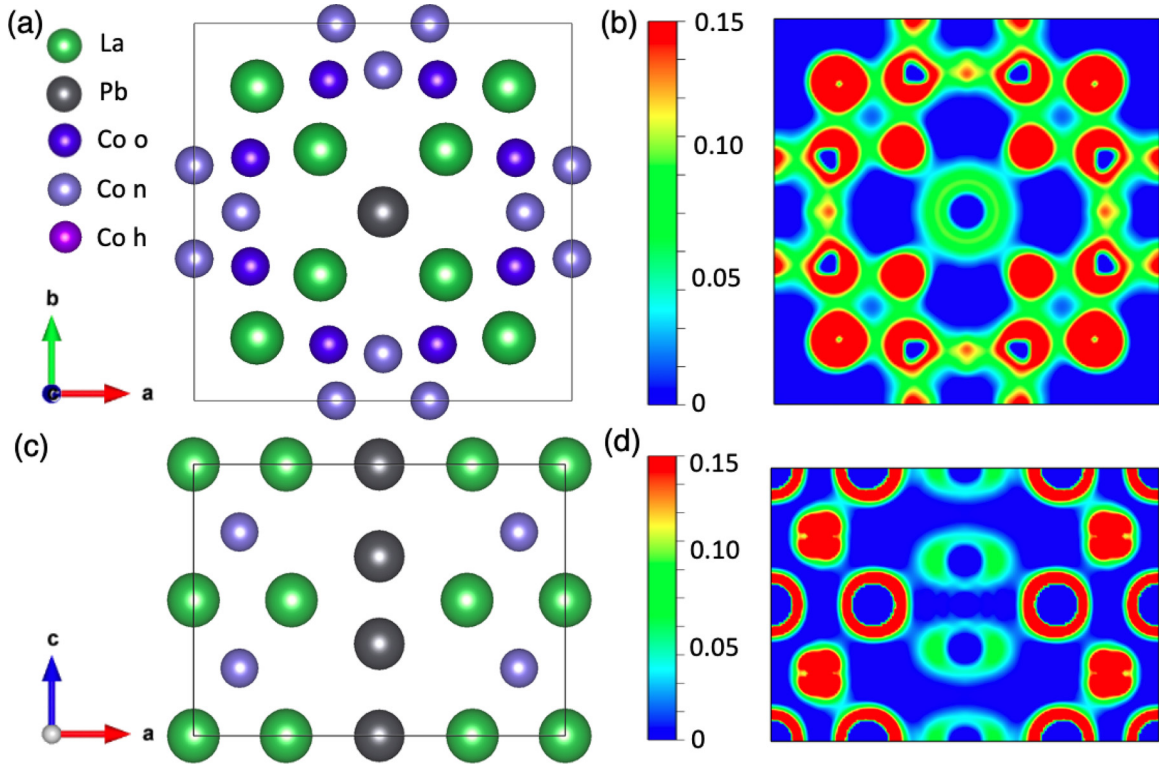


FIG. 3. The atomic positions (a) and the differential charge density (b) in the ab plane cutting through the center Pb atom, and the atomic positions (c) and the differential charge density (d) in the ac plane cutting through the center Pb atom, in the ground state FM $\text{La}_{18}\text{Co}_{28}\text{Pb}_3$ compound.

orbitals. These observations agree with Fig. 4(d) in that the major difference comes from Co o and n sites.

Next, by employing constraining moment calculations we study the shape of the adiabatic energy surface between the obtained spin states of $\text{La}_{18}\text{Co}_{28}\text{Pb}_3$. In Fig. 5, the possible path between the low and high spin states is shown as a function of the total moment. The constrained magnetic moment calculations are performed by adopting the scheme from [21] implemented in VASP. In particular, the initial moments on each nonequivalent Co site are confined along the out-of-plane, easy direction with the lowest energy. At each constraint, as shown in Fig. 5, the ratios of the moments on the three nonequivalent Co sites are kept the same as those at the equilibrium volume for the low spin (blue) or high spin (red) calculation, respectively. The weight λ of the penalty function is set to 20 for all calculations, and the calculated total energies are converged within 10^{-5} eV per magnetic atom. The Wigner-Seitz radius of each atom is chosen so that the sum of the volume of the spheres is equal to the volume of the cell. With such a simple static constraint, we found two FM states with the transition around the averaged moment of $0.3 \mu_B$. The magnetic adiabatic surface resembles an asymmetric double potential with very low barrier energy (< 1 meV/atom) from the low spin to the high spin state. The existence of such potential in the “classical” spin energy would lead to the appearance of the quantum spin tunneling effect.

We estimated this tunneling by employing the *ab initio* spin instanton technique [22], which is implemented in the tight-binding linear muffin-tin-orbital method.

The tunneling splitting is written as $\Delta(\tau) = \frac{2\hbar\omega_0 T_0}{\pi} e^{\omega_0 \tau - 2S_M}$, where $\hbar\omega_0$ is the initial time dependence of the kinetic energy, S_M is a magnetic contribution to the effective action, τ is a time to reach the low spin state, and T_0 is the initial kinetic energy (used as a trial value). Starting from the high-spin initial configuration, spin instanton dynamics was performed for ten different T_0 in the range 0.001–0.1 meV. For each value of T_0 , the corresponding initial spin deviation angle was determined by trial and error. Time steps of 0.11 a.u. ($1 \text{ a.u.} = 2.418884326509 \times 10^{-17} \text{ s}$) were used. The resulting splittings appear to be in the range of 0.08–0.1 meV/atom and cannot affect the relative stability of the high spin state.

It is worth noting that the DOS of the ground state plotted in Fig. 2(b) shows that the Co d states in this compound exhibit a somewhat narrow bandwidth of ~ 3 eV compared to 4–4.5 eV in the elemental hcp Co. This could suggest somewhat stronger electronic correlations in this system. We check the sensitivity of the calculated electronic structure and magnetic properties of $\text{La}_{18}\text{Co}_{28}\text{Pb}_3$ to the variations of possible atomic Coulomb correlations by performing DFT+ U calculations. Adding the U term on Co atoms in DFT-PBE calculations, we found the magnetic moments of the Co atoms increase significantly and almost linearly with the value of U in the range of 0–4 eV (Fig. 6). Whether DFT+ U should be used, and which U value should be used in the DFT+ U calculation for an accurate description of magnetization in this compound remains an open question for future investigations.

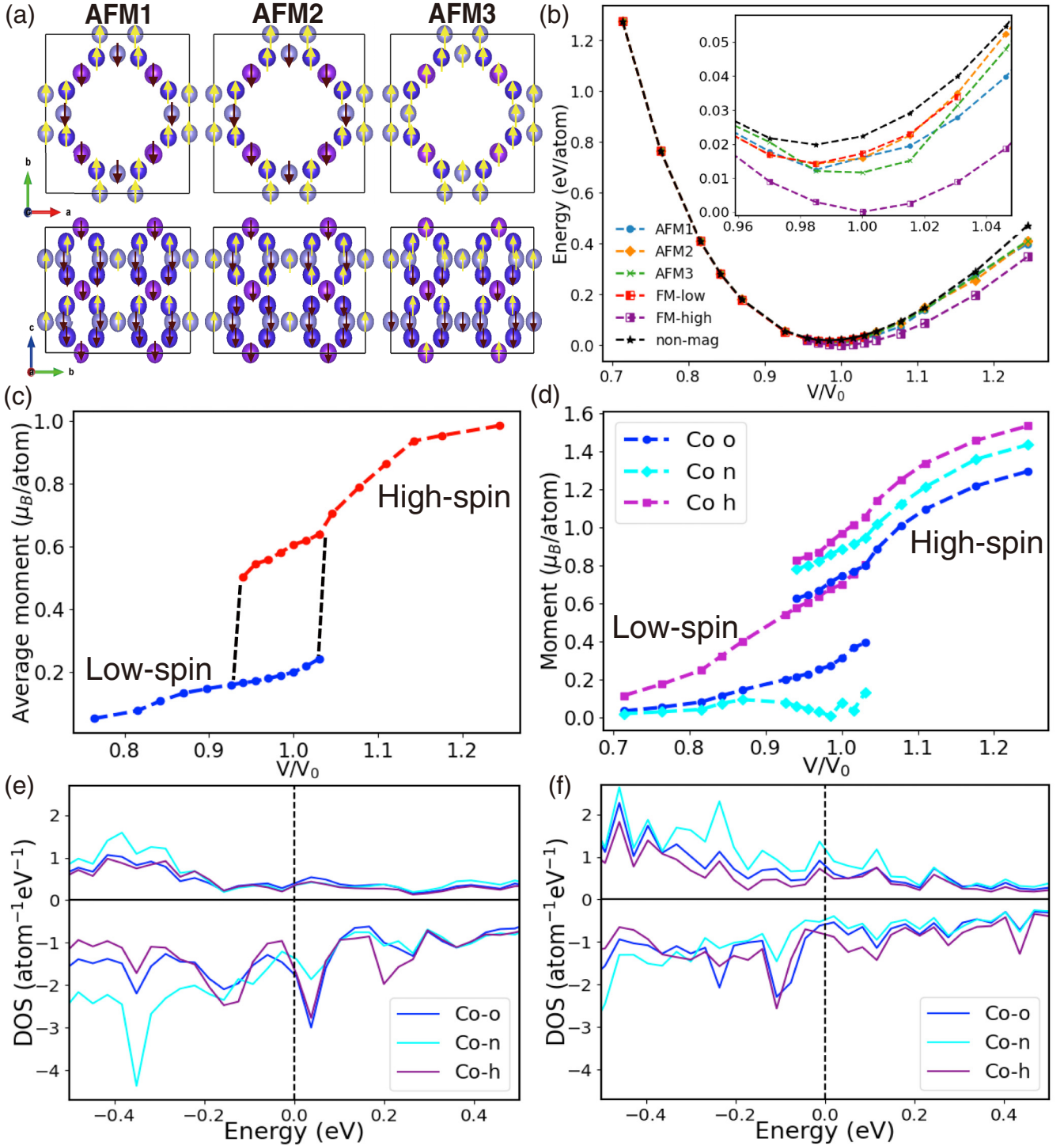


FIG. 4. (a) Illustration of three AFM configurations. Nonequivalent Co atoms are colored differently from previous figures. Left: $a-b$ in-plane AFM configuration (AFM1); middle: another $a-b$ in-plane AFM configuration (AFM2); right: out-of-plane AFM configuration (AFM3). (b) The total energy per Co atom as the function of volume change (V/V_0) for various states. (c) The averaged magnetic moment per Co atom in the two FM phases in $\text{La}_{18}\text{Co}_{28}\text{Pb}_3$ calculated at different V/V_0 . (d) The atomic decomposed magnetic moments for the nonequivalent Co atoms at different V/V_0 . (e), (f) The decomposed DOS per atom for the nonequivalent Co atoms in high spin (e) and low spin (f) state at the equilibrium volume V_0 .

IV. STONER AND CURIE TEMPERATURES

Next, we evaluate the Stoner temperatures of the low- and high-spin FM magnetic phases of the $\text{La}_{18}\text{Co}_{28}\text{Pb}_3$ com-

pound. Figure 7 shows the unit cell's magnetization as the electronic temperature function for the two FM phases. The Stoner temperature is defined as the electronic temperature above which the magnetic moment of the compound vanishes.

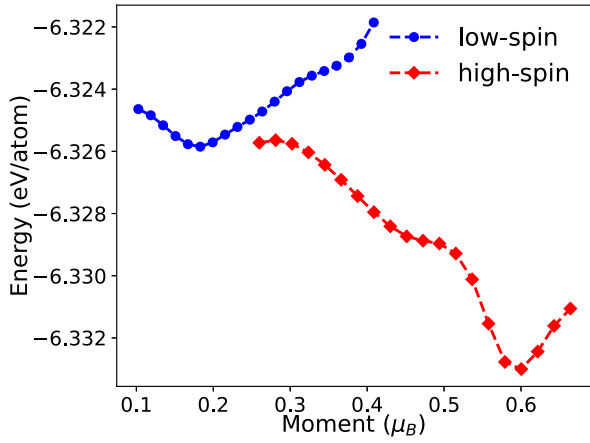


FIG. 5. Asymmetric double-well potential energy surface between low and high spin states in $\text{La}_{18}\text{Co}_{28}\text{Pb}_3$. The directions of the initial moments on each nonequivalent Co site are constrained in out-of-plane direction in the calculation, and the ratios of these moments are kept the same as those at the equilibrium volume, for the low spin (blue) or high spin (red) calculation, respectively.

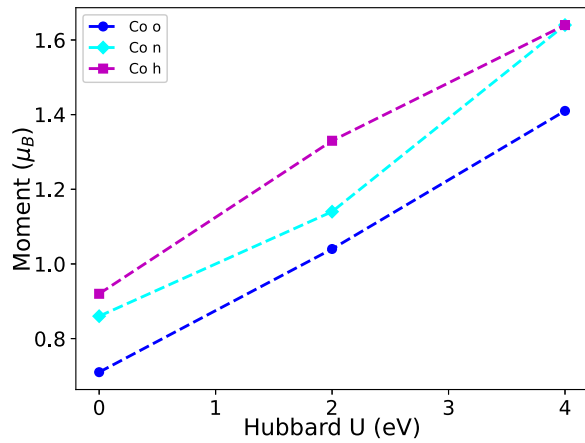


FIG. 6. The calculated magnetic moments for different Co sites in $\text{La}_{18}\text{Co}_{28}\text{Pb}_3$ as a function of the Hubbard U parameter on Co atoms.

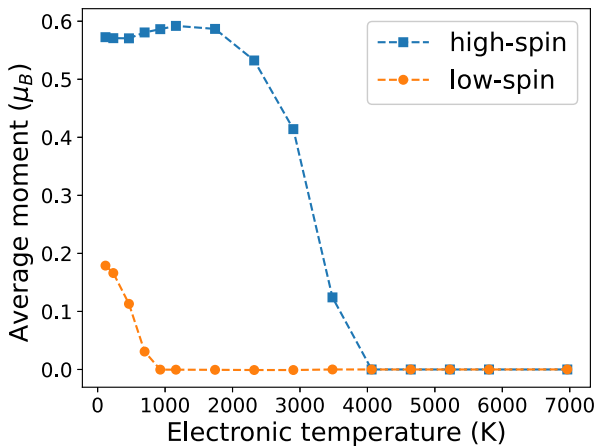


FIG. 7. The calculated Stoner temperature of both high-spin and low-spin FM states of $\text{La}_{18}\text{Co}_{28}\text{Pb}_3$.

From Fig. 7, we can see that the Stoner temperature of the low-spin FM phase is about 900 K. In contrast, the high-spin FM phase can be as high as 4000 K. These results suggest that the Stoner model is unsuitable for our system's localized high-spin FM state. Instead, the Heisenberg model could be more relevant in this case. Within the framework of the Heisenberg model, the Curie temperature T_c can be estimated using the mean-field approximation, which involves calculating the energy difference between the FM and AFM configurations. The mean-field expression $T_c \sim \frac{2}{3}J_0$, where J_0 is the effective exchange interaction parameter evaluated from the difference $E_{\text{AFM}} - E_{\text{FM}}$. The T_c for the high-spin FM state appears to be around 60 K, supporting the possible coexistence of two FM states below 60 K.

Alternatively, we can estimate the Curie temperature from the paramagnetic (high-temperature) limit. To do this, we first obtain the free energy of magnetic systems with thermal spin fluctuations due to Bose-Einstein excitations (absent in $T = 0$ K, DFT) using the coupling constant integration [14,17,23–25] of a spin-disordered state. The details of the susceptibility calculations can be found in [26]. It is clear from Fig. 7 that we can safely calculate spin paramagnetic susceptibility below 2000 K for the high spin state where magnetic moments on the Co atom still look localized enough. For such high-temperature cases, we obtain the susceptibility

$$\chi(\mathbf{q}) = \frac{\chi_0(\mathbf{q})}{1 - (I - \lambda)\chi_0(\mathbf{q})}, \quad (1)$$

where for the Moriya-Kawabata parameter

$$\lambda(T) = 3kT \int_0^I dI \sum_{\mathbf{q}} [\chi(\mathbf{q}) - \chi_0(\mathbf{q})]. \quad (2)$$

Our calculations indeed revealed a linear dependence of inverse susceptibility below 1300 K, which can be fitted with the traditional expression

$$\chi(\mathbf{q} = 0) = \frac{\mu_{\text{eff}}^2}{3(T - T_c)} \quad (3)$$

to extract the high-temperature effective moments. For the average effective moment μ_{eff} , we obtained a value of $1.8\mu_B$ with the critical temperature of magnetic phase transition $T_c = 145$ K. We believe this estimate is more reliable than the mean-field values obtained above due to the presence of large itineracy.

We also note that the degree of localization of the magnetic moment and the Curie temperature strongly depend on the moment's amplitude. As shown in Fig. 6, the magnetic moments of the Co atoms increased when the Hubbard parameter U was added. Therefore, the estimated Curie temperature is also subject to change with U . Our DFT+ U calculation using $U = 2$ eV produces a much higher mean-field estimate T_c of about 540 K with $\mu_{\text{eff}} = 2.1\mu_B$. We expect an even larger T_c for larger U values, but such strong correlations could be unlikely for this system. In any case, all obtained numbers, and especially the strong sensitivity of the results to the value of the Hubbard parameter in this metallic system, should be easily verified experimentally when samples are available. Overall, the “enhancement” of magnetism due to the introduction of Hubbard U is significant for both the T_c and effective

moments. The T_c increase is unusually large and relatively rare. These results would suggest that this system is at the borderline of magnetic instability; not only Hubbard parameters but also pressure, field, and so on can have significant effects on the magnetic behavior of the system.

V. SUMMARY

In summary, we investigated the electronic and magnetic properties of the recently predicted $\text{La}_{18}\text{Co}_{28}\text{Pb}_3$ compound containing an immiscible pair of elements Co and Pb. The DFT-PBE calculations predicted an FM state as the ground state. Our study also revealed the coexistence of high- and low-spin magnetic states in the extensive range of volumes that can be accessed experimentally. The spin tunneling effect between these two states using the spin instanton technique appears to be relatively small and cannot influence the stability of the ground state. The calculations of the temperature-dependent susceptibility using integration over the parameter method produced a Curie temperature of about 145 K. We further predicted a strong dependence of the Curie temperature and the paramagnetic moment on the strength of Hubbard-type correlations. Further experimental research is needed to verify our predictions. Despite several attempts [13], it is still a great challenge to make a single phase of this compound for experimental measurements of its magnetic properties.

New crystallographic data for $\text{La}_{18}\text{Co}_{28}\text{Pb}_3$ are made available to the public through our ML-materials database [27]. The other data that support the findings of this paper, including both experimental and computational results, are available from the contact author upon reasonable request. All codes used in this work are accessible through their websites. We use VASP 5.4.1 version in this work.

ACKNOWLEDGMENTS

We are grateful to Prof. Paul Canfield for his insightful suggestion on exploring the structures and properties of ternary La-Co-Pb compounds, which contain a pair of immiscible elements Co and Pb, and to Dr. Tyler Slade for discussions and his great effort in the experimental synthesis of La-Co-Pb ternary compounds. We also acknowledge insightful discussions with Dr. Feng Zhang on theoretical calculations. Work at Ames Laboratory was supported by the U.S. Department of Energy (DOE), Office of Science, Basic Energy Sciences, Materials Science and Engineering Division, including a grant of computer time at the National Energy Research Supercomputing Center (NERSC) in Berkeley. Ames Laboratory is operated for the U.S. DOE by Iowa State University under Contract No. DE-AC02-07CH11358.

The authors declare no competing interests.

-
- [1] J. A. Hertz, Quantum critical phenomena, *Phys. Rev. B*, **14**, 1165 (1976).
 - [2] G. D. Samolyuk and V. P. Antropov, Character of magnetic instabilities in CaFe_2As_2 , *Phys. Rev. B* **79**, 052505 (2009).
 - [3] Y. Takahashi, *Spin Fluctuation Theory of Itinerant Electron Magnetism*, Springer Tracts in Modern Physics (Springer-Verlag, Berlin, Heidelberg, 2013), Vol. 253.
 - [4] S. N. Kaul, Spin-fluctuation theory for weak itinerant-electron ferromagnets: revisited, *J. Phys.: Condens. Matter* **11**, 7597 (1999).
 - [5] G. G. Lonzarich and L. Taillefer, Effect of spin fluctuations on the magnetic equation of state of ferromagnetic or nearly ferromagnetic metals, *J. Phys. C: Solid State Phys.* **18**, 4339 (1985).
 - [6] T. Moriya and K. Ueda, Spin fluctuations and high temperature superconductivity, *Adv. Phys.* **49**, 555 (2000).
 - [7] D. C. Johnston, The puzzle of high-temperature superconductivity in layered iron pnictides and chalcogenides, *Adv. Phys.* **59**, 803 (2010).
 - [8] K. Held, Electronic structure calculations using dynamical mean field theory, *Adv. Phys.* **56**, 829 (2007).
 - [9] P. C. Canfield, New materials physics, *Rep. Prog. Phys.* **83**, 016501 (2019).
 - [10] P. C. Canfield and S. L. Bud'ko, FeAs-based superconductivity: A case study of the effects of transition metal doping on BaFe_2As_2 , *Annu. Rev. Condens. Matter Phys.* **1**, 27 (2010).
 - [11] U. S. Kaluarachchi, S. L. Bud'ko, P. C. Canfield, and V. Taufour, Tricritical wings and modulated magnetic phases in LaCrGe_3 under pressure, *Nat. Commun.* **8**, 546 (2017).
 - [12] V. Taufour, U. S. Kaluarachchi, R. Khasanov, M. C. Nguyen, Z. Guguchia, P. K. Biswas, P. Bonfà, R. D. Renzi, X. Lin, S. K. Kim, E. D. Mun, H. Kim, Y. Furukawa, C.-Z. Wang, K.-M. Ho, S. L. Bud'ko, and P. C. Canfield, Ferromagnetic quantum critical point avoided by the appearance of another magnetic phase in LaCrGe_3 under pressure, *Phys. Rev. Lett.* **117**, 037207 (2016).
 - [13] R. Wang, W. Xia, T. J. Slade, X. Fan, H. Dong, K.-M. Ho, P. C. Canfield, and C.-Z. Wang, Machine learning guided discovery of ternary compounds involving La and immiscible Co and Pb elements, *npj Comput. Mater.* **8**, 258 (2022).
 - [14] Y. Sun, K.-M. Ho, and V. P. Antropov, Metallization and spin fluctuations in Cu-doped lead apatite, *Phys. Rev. Mater.* **7**, 114804 (2023).
 - [15] A. Aguayo, I. I. Mazin, and D. J. Singh, Why Ni_3Al is an itinerant ferromagnet but Ni_3Ga is not, *Phys. Rev. Lett.* **92**, 147201 (2004).
 - [16] V. P. Antropov and A. Solontsov, The influence of quantum spin fluctuations on magnetic instability, *J. Appl. Phys.* **109**, 07E116 (2011).
 - [17] R. Wang, Y. Sun, V. Antropov, Z. Lin, C.-Z. Wang, and K.-M. Ho, Theoretical prediction of a highly responsive material: Spin fluctuations and superconductivity in FeNiB_2 system, *Appl. Phys. Lett.* **115**, 182601 (2019).
 - [18] J. P. Perdew, K. Burke, and M. Ernzerhof, Generalized gradient approximation made simple, *Phys. Rev. Lett.* **77**, 3865 (1996).
 - [19] G. Kresse and J. Furthmüller, Efficiency of *ab-initio* total energy calculations for metals and semiconductors using a plane-wave basis set, *Comput. Mater. Sci.* **6**, 15 (1996).

- [20] G. Kresse and J. Furthmüller, Efficient iterative schemes for *ab initio* total-energy calculations using a plane-wave basis set, *Phys. Rev. B* **54**, 11169 (1996).
- [21] P.-W. Ma and S. L. Dudarev, Constrained density functional for noncollinear magnetism, *Phys. Rev. B* **91**, 054420 (2015).
- [22] M. I. Katsnelson, M. van Schilfgaarde, V. P. Antropov, and B. N. Harmon, *Ab initio* instanton molecular dynamics for the description of tunneling phenomena, *Phys. Rev. A* **54**, 4802 (1996).
- [23] T. Izuyama and R. Kubo, Some considerations on the magnetic carriers in ferromagnetic transition metals, *J. Appl. Phys.* **35**, 1074 (1964).
- [24] T. Moriya and A. Kawabata, Effect of spin fluctuations on itinerant electron ferromagnetism, *J. Phys. Soc. Jpn.* **34**, 639 (1973).
- [25] A. Kawabata, Interaction of spin fluctuations in ferromagnetic and nearly ferromagnetic itinerant systems, *J. Phys. Met. F* **4**, 1477 (1974).
- [26] A. L. Wysocki, V. N. Valmispild, A. Kutepov, S. Sharma, J. K. Dewhurst, E. K. U. Gross, A. I. Lichtenstein, and V. P. Antropov, Spin-density fluctuations and the fluctuation-dissipation theorem in 3d ferromagnetic metals, *Phys. Rev. B* **96**, 184418 (2017).
- [27] <https://ml-material.physics.iastate.edu/database>.